Two-Color Pump−Probe Spectroscopies of Two- and Three-Level Systems: 2-Dimensional Line Shapes and Solvation Dynamics

Kijeong Kwac and Minhaeng Cho*

Department of Chemistry and Center for Multidimensional Spectroscopy, Division of Chemistry and Molecular Engineering, Korea University, Seoul 136-701, Korea

Received: March 20, 2003; In Final Form: May 24, 2003

For both two- and three-level systems, theoretical descriptions of two-color transient grating, transient dichroism, and transient birefringence spectroscopies were presented. The two-dimensional line shapes of these pump−probe spectra were found to be strongly dependent on the solvation dynamics. The two-dimensional contours of the transient birefringence signal of a two-level system are not vertically directed in the short time region. The inverse slope of the tangential line of the two-dimensional contours was found to be linearly proportional to the solvation correlation function. The two-dimensional transient grating and dichroism spectra are shown to directly provide quantitative information on the reorganization energy and spectral diffusion dynamics. For a three-level system that is a model for an anharmonic oscillator, the peak separation observed in a two-dimensional transient dichroism spectrum was found to be determined by both fluctuation amplitude of the transition frequency and spectral bandwidth of the probe pulse. The transient dichroism and birefringence contours of a three-level system were also found to be tilted in the short time region. We, in the present paper, established a variety of relationships between two-dimensional pump−probe line shapes and solvation correlation function.

I. Introduction

Transient grating spectroscopy has been used to study wave packet (particle and hole) evolutions on the excited and ground states.[1−7] By injecting two simultaneously propagating laser pulses with different wave vectors, vibrational coherence states, hole and particle, are created on the ground and excited states, respectively. A probe laser pulse delayed from the pump pulses is used to create a third-order polarization in the optical sample. Then, generated signal field intensity is measured in the case of the transient grating experiment. For a two-electronic-level system, the population relaxation and the electronic dephasing process induced by fluctuating chromophore-solvent interaction energy can therefore be studied with this TG method. Other methods to study the time evolution of the same third-order polarization are transient dichroism (TD) and transient birefringence (TB) measurements. Instead of detecting signal field intensity, an experimentalist can control the phase of the local oscillator to measure either the imaginary or real parts of the third-order polarization. These correspond to the TD and TB experiments. All of these three different spectroscopies will be referred to as pump−probe spectroscopies in general.

In the present paper, we will consider two-color (2-C) pump−probe (PP) spectroscopy, where the pump and probe frequencies are different from each other. In this case, the initial particle and hole wave packets or doorway states, created by the two field-matter interactions with the pump, are located at different region of phase space of the window specified by the width and frequency of the probe pulse. On the other hand, in the case of the conventional 1-C PP, the phase space region of the initial wave packet is identical with that of the window. Therefore, 1-C PP measures how rapidly the initial wave packet moves away from the initial phase space region in time so that the 1-C TG signal decays monotonically. In contrast, due to the difference between the doorway phase space and the window phase space, the 2-C TG signal rises initially and reaches a maximum value at the time when the propagating wave packet passes through the window phase space, as experimentally observed by Fleming and co-workers.[8] Because of this additional experimental controllability of the 2-C PP, it becomes possible to explore a much wider region of the phase space spanned by the coupled bath degrees of freedom.

The 2-C PP spectroscopies, because of their dependencies on both pump and probe frequencies, are time- and frequency-resolved two-dimensional (2-D) spectroscopies. The fifth-order three-pulse scattering spectroscopy theoretically proposed by Cho and Fleming[9] was the early version of temporally resolved two-dimensional electronic spectroscopy. Jonas and co-workers[10] demonstrated that a 2-D electronic spectroscopy based on a four-wave-mixing scheme is experimentally feasible and showed that the diagonal elongation of the 2-D contours is a signature of the inhomogeneous contribution to the line broadening. Tokmakoff[11] studied the 2-D line shapes for a few limiting cases, either Lorentzian or Gaussian limits, and particularly he showed that the 2-D spectral profiles along the diagonal and anti-diagonal axes are strongly dependent on the detailed line broadening mechanisms, though the 1-D line shape is rather insensitive to them.

Recently, Hamm and co-workers[12,13] used the 2-D IR PP spectroscopy to investigate the role of solvation dynamics on the 2-D contour line shapes of the amide I band from aqueous *N*-methylacetamide (NMA) and trialanine solutions. They found that the 2-D contours are not vertically directed in the short time domain and become vertically directed after 4 ps. The physics behind this phenomenon can be understood by noting the fact that the chromophore−solvent dynamics is not a

* To whom correspondence should be addressed. E-mail address: mcho@korea.ac.kr.

10.1021/jp034727w CCC: $25.00
Published on Web 07/10/2003

Markovian process. In other words, the memory about the initial transition frequency lasts at least for 4 ps. Consequently, any dynamical or chemical processes occurring in less than 4 ps would experience inhomogeneous solvent environments. To clarify the solvation effects on the 2-D PP spectra of NMA in liquid water, we carried out molecular dynamics simulations in combination with ab initio calculations and showed that the librational and hindered translational motions of surrounding water molecules are critical in determining amide I mode frequency fluctuation amplitude and time scale of the memory loss rate mentioned above.[14] Furthermore, we proved that the degree of slant of the 2-D contours is linearly proportional to the solvation correlation function.[14] This observation is particularly interesting because the early part of the solvation correlation function can be accurately determined by examining the time-evolution of 2-D TD contours. This is in contrast with the photon echo peak shift measurement technique,[15] though it is one of the most effective ways to determine the slowly decaying part of the solvation dynamics and to estimate the magnitude of static inhomogeneity in glassy materials.

In this paper, we will present theoretical descriptions of six different cases of pump−probe spectroscopies, i.e., (1) 2-C TG of a 2-level system, (2) 2-C TD of a 2-level system, (3) 2-C TB of a 2-level system, (4) 2-C TG of a 3-level system, (5) 2-C TD of a 3-level system, and (6) 2-C TB of a 3-level system. In ref 14, we considered only the fifth case in an impulsive pulse limit. Therefore, a finite pulse width effect on the 2-C TD signal of a three-vibrational-level system was not taken into account correctly, though it was for the first time found that the inverse slope of 2D TD contours is directly related to the solvation correlation function. Mukamel and co-workers studied the second case, one-dimensional TD of a 2-level system in the high-temperature limit.[16] In section II, theoretical descriptions of 2-C TG, TD, and TB signals of a two-level system will be presented. Numerical calculation results for a model system will be discussed in section III. In section IV, the theory in section II will be extended to a three-vibrational-level system and numerically calculated 2-C TG, TD, and TB spectra as a function of the pump−probe delay time will be presented. Finally, in section V, the main results will be summarized.

II. Theoretical

In the present section, we will first consider a two-level system that is an excellent model for a dye molecule interacting with optical (visible or UV) fields, whereas a three-level system that is a model for a weakly anharmonic oscillator interacting with multiple IR fields will be considered in section IV. Depending on the experimental scheme, one can measure real or imaginary parts of the third-order material polarization or its intensity. The so-called transient grating measurement utilizes two pulses with wave vectors of k_1 and k_2. Then, the third ($\boldsymbol{k}_3$) pulse which is delayed in time is injected, and the scattered signal field intensity in the direction of $-k_1 + k_2 + k_3$ is detected (homodyne detection). The self-heterodyned pump−probe spectroscopy, on the other hand, uses a single pump pulse with wave vector of k_1, and the k_2 probe pulse delayed in time is injected to create the corresponding third-order polarization and the interference of the material signal field with the probe field is measured. Therefore, the pump−probe signal in this case is linearly proportional to the material polarization, particularly the imaginary part of the polarization. If the phase of a local oscillator field could further be controlled, one could measure either the real or imaginary parts of the polarization separately, which correspond to TB and TD, respectively. In any case, the third-order nonlinear response function associated with the three different experiments, i.e., TG, TD, and TB spectroscopies, are all the same.

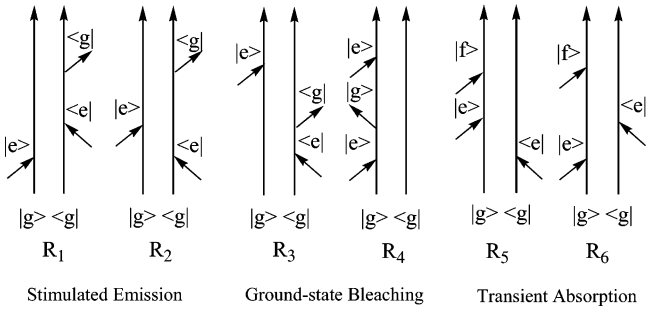

Figure 1. Six double-sided Feynman diagrams. The first two involves time-evolution of the particle on the excited state, whereas the second two (R_3 and R_4) describes hole dynamics on the ground-state potential energy surface. The final two (R_5 and R_6) are associated with the transition absorption from the first excited state $|e\rangle$ to the second excited state $|f\rangle$.

The frequencies of the pump and probe fields will be denoted as ω_{pu} and ω_{pr}, respectively. The third-order polarization is given as[16]

$$P^{(3)}(k_s, t) = \left(\frac{i}{\hbar}\right)^3 \int_0^\infty dt_1 \int_0^\infty dt_2 \int_0^\infty dt_3\, [R_1 + R_4] E_{pr}(t - t_3) E_{pu}^*(t + \tau - t_3 - t_2)\, E_{pu}(t + \tau - t_3 - t_2 - t_1) \exp(i\omega_{pr} t_3 + i\omega_{pu} t_1) + \int_0^\infty dt_1 \int_0^\infty dt_2 \int_0^\infty dt_3\, [R_2 + R_3] E_{pr}(t - t_3) E_{pu}(t + \tau - t_3 - t_2)\, E_{pu}^*(t + \tau - t_3 - t_2 - t_1) \exp(i\omega_{pr} t_3 - i\omega_{pu} t_1) \quad (1)$$

Here, the pulse envelopes were denoted as E_m (m = pu or pr). Throughout this paper, we will consider the case when the pump and probe pulses are well separated in time. Four response function components, R_j ($j = 1 \sim 4$), will be discussed in detail in the following subsection. The homodyne-detected TG signal and the heterodyne-detected pump probe (HD-PP) signal are[17]

$$S_{TG}(\omega_{pu}, \omega_{pr}; \tau) = \int_{-\infty}^\infty dt\, |P^{(3)}(k_s, t)|^2$$

$$S_{HD-PP}(\omega_{pu}, \omega_{pr}; \tau; \phi) = \mathrm{Im}[e^{i\phi} \int_{-\infty}^\infty dt\, E_{LO}^*(k_{LO}, t) P^{(3)}(k_s, t)] \quad (2)$$

The phase of the local oscillator (LO), ϕ, can be controlled to be zero or $\pi/2$, and then $S_{HD-PP}(\omega_{pu}, \omega_{pr}; \tau; \phi = 0)$ and $S_{HD-PP}(\omega_{pu}, \omega_{pr}; \tau; \phi = \pi/2)$ correspond to the TD and the TB signals, respectively.

Now, let us introduce a new integration variable $t' = t + \tau - t_3 - t_2$ and assume that the delay time τ is sufficiently larger than the pulse width. Then, we have

$$P^{(3)}(k_s, t) = \left(\frac{i}{\hbar}\right)^3 \int_0^\infty dt_1 \int_{-\infty}^\infty dt' \int_0^\infty dt_3\, E_{pr}(t - t_3) E_{pu}^*(t') E_{pu}(t' - t_1) \{(R_1 + R_4) \exp[i\omega_{pr} t_3 + i\omega_{pu} t_1] + (R_2 + R_3) \exp[i\omega_{pr} t_3 - i\omega_{pu} t_1]\} \quad (3)$$

Later, eq 3 will be used to derive approximate expression for $P^{(3)}(k_s, t)$.

A. Short-Time Approximations. The general nonlinear response function of a two-level system was presented before and is given by a sum of the following four components (see Figure 1 for the corresponding double-sided Feynman diagrams) and their complex conjugates[16]

$$R_1(t_3, t_2, t_1) = \langle \mu_{eg}{}^4 \rangle \exp(-i\omega_{eg}t_1 - i\omega_{eg}t_3) \exp\{-g^*(t_3) - g(t_1) - f_+(t_3, t_2, t_1)\}$$

$$R_2(t_3, t_2, t_1) = \langle \mu_{eg}{}^4 \rangle \exp(i\omega_{eg}t_1 - i\omega_{eg}t_3) \exp\{-g^*(t_3) - g^*(t_1) + f_+^*(t_3, t_2, t_1)\}$$

$$R_3(t_3, t_2, t_1) = \langle \mu_{eg}{}^4 \rangle \exp(i\omega_{eg}t_1 - i\omega_{eg}t_3) \exp\{-g(t_3) - g^*(t_1) + f_-^*(t_3, t_2, t_1)\}$$

$$R_4(t_3, t_2, t_1) = \langle \mu_{eg}{}^4 \rangle \exp(-i\omega_{eg}t_1 - i\omega_{eg}t_3) \exp\{-g(t_3) - g(t_1) - f_-(t_3, t_2, t_1)\} \quad (4)$$

where the two auxiliary functions are defined as

$$f_+(t_3, t_2, t_1) = g^*(t_2) - g^*(t_2 + t_3) - g(t_1 + t_2) + g(t_1 + t_2 + t_3)$$

$$f_-(t_3, t_2, t_1) = g(t_2) - g(t_2 + t_3) - g(t_1 + t_2) + g(t_1 + t_2 + t_3) \quad (5)$$

Here, the line broadening function, $g(t)$, is given as

$$g(t) \equiv \int_0^t d\tau_1 \int_0^{\tau_1} d\tau_2 \, \xi_{ee}(\tau_2) \quad (6)$$

where the linear correlation function of the fluctuating transition frequency between $|e\rangle$ and $|g\rangle$ is

$$\xi_{ee}(\tau_2) = \langle \delta\omega_{eg}(\tau_2)\delta\omega_{eg}(0)\rangle \quad (7)$$

The above line broadening function, $g(t)$, can be rewritten as[18]

$$g(t) = -i\frac{\lambda}{\hbar}t + \int_0^\infty d\omega \, \rho(\omega) \coth\left[\frac{\hbar\omega\beta}{2}\right](1 - \cos\omega t) + i\int_0^\infty d\omega \, \rho(\omega) \sin\omega t \quad (8)$$

where the spectral density $\rho(\omega)$ represents system-bath coupling strengths and frequency distribution of the coupled bath modes. $\beta = 1/k_BT$ where k_B and T are the Boltzmann constant and the temperature, respectively. Orientational average of the transition dipole product was denoted as $\langle \mu_{eg}{}^4 \rangle$ in eq 4.

Noting that the electronic coherence relaxation times during the t_1 and t_3 period are typically very short and assuming that $t_2 \cong \tau$ and $t_1 + t_2 \cong \tau$, one can use second-order truncated Taylor expansion forms of various $g(t)$ functions in eqs 5 so that we have

$$f_+ \cong 2iQ(\tau)t_3 + H(\tau)t_1t_3$$
$$f_- \cong H(\tau)t_1t_3 \quad (9)$$

where

$$Q(\tau) \equiv \left(S(\tau) - \frac{\lambda}{\hbar}\right) \quad (10)$$

$$H(\tau) \equiv \int_0^\infty d\omega \, \rho(\omega) \coth\left[\frac{\hbar\omega\beta}{2}\right]\omega^2 \cos\omega\tau \quad (11)$$

$$S(\tau) \equiv \int_0^\infty d\omega \, \rho(\omega) \, \omega \cos\omega\tau \quad (12)$$

Here, the solvation correlation function was denoted as $S(\tau)$ and the auxiliary function $Q(\tau)$ is linearly proportional to $S(\tau)$. The solvent reorganization energy λ is defined as[18]

$$\lambda \equiv \hbar\int_0^\infty d\omega \, \rho(\omega) \, \omega \quad (13)$$

In the high-temperature limit, $H(\tau)$ is linearly proportional to the solvation correlation function as

$$H(\tau) \cong \frac{2}{\hbar\beta}\int_0^\infty d\omega \, \rho(\omega) \, \omega \cos\omega\tau = \frac{2}{\hbar\beta}S(\tau) \quad (14)$$

Also, using a short-time approximation to $g(t)$ with respect to t_1 and t_3, we have

$$g(t_1) = g^*(t_1) \cong \frac{1}{2}\Omega^2 t_1{}^2 \quad \text{and} \quad g(t_3) = g^*(t_3) \cong \frac{1}{2}\Omega^2 t_3{}^2 \quad (15)$$

where the mean square fluctuation amplitude of the electronic transition frequency is defined as

$$\Omega^2 \equiv \int d\omega \, \rho(\omega) \, \omega^2 \coth\frac{\hbar\omega\beta}{2} \quad (16)$$

In the high-temperature limit, $\Omega^2 \cong 2/\hbar\beta \int d\omega \, \rho(\omega) \, \omega = 2\lambda/\hbar^2\beta$.

Thus, the four response function components in eq 4 can be simplified as[15,19,20]

$$R_1(t_3, \tau, t_1) = \exp(-i\omega_{eg}t_1 - i\omega_{eg}t_3) \exp\left\{-\frac{1}{2}\Omega^2 t_1{}^2 - \frac{1}{2}\Omega^2 t_3{}^2 - 2iQ(\tau)t_3 - H(\tau)t_1t_3\right\}$$

$$R_2(t_3, \tau, t_1) = \exp(i\omega_{eg}t_1 - i\omega_{eg}t_3) \exp\left\{-\frac{1}{2}\Omega^2 t_1{}^2 - \frac{1}{2}\Omega^2 t_3{}^2 - 2iQ(\tau)t_3 + H(\tau)t_1t_3\right\}$$

$$R_3(t_3, \tau, t_1) = \exp(i\omega_{eg}t_1 - i\omega_{eg}t_3) \exp\left\{-\frac{1}{2}\Omega^2 t_1{}^2 - \frac{1}{2}\Omega^2 t_3{}^2 + H(\tau)t_1t_3\right\}$$

$$R_4(t_3, \tau, t_1) = \exp(-i\omega_{eg}t_1 - i\omega_{eg}t_3) \exp\left\{-\frac{1}{2}\Omega^2 t_1{}^2 - \frac{1}{2}\Omega^2 t_3{}^2 - H(\tau)t_1t_3\right\} \quad (17)$$

Because the first two response function components, R_1 and R_2, describe the time-evolution of a particle on the excited state, spectral diffusion contribution plays a crucial role, as manifest by the term, $\exp\{-2iQ(\tau)t_3\}$, whereas there are no such contributions to R_3 and R_4. This does not mean that a hole created on the ground state does not undergo a spectral diffusion, as will be shown in the following subsection. In the literatures, the first two contributions, R_1 and R_2, were referred to as stimulated emission (SE) term and the last two contributions, R_3 and R_4, were as ground-state bleaching (GB) term. Because of the cross terms such as $\pm H(\tau)t_1t_3$ in eqs 17, the memory on the initially created particle or hole wave packets on the excited or ground states, respectively, which can survive over the population evolution period, was approximately taken into account in eqs 17.

B. 2-Dimensional Polarization Function: Two-Level System. To take into account the finite pulse width effect on the 2-C PP signals, the pulse envelope functions are assumed to be a Gaussian form as $E_{pu}(t) = \exp(-w^2t^2/2)$ and $E_{pr}(t) = \exp(-\bar{w}^2t^2/2)$. Inserting Gaussian pulse envelope functions into eq 3, replacing $R_j(t_3, t_2, t_1)$ in eq 3 with $R_j(t_3, \tau, t_1)$ in eqs 17, and carrying out multiple integrals with the approximations

stated above eq 9, we find that the total polarization is given by a sum of two contributions, $P^{(3)}_{SE}(k_s, t)$ and $P^{(3)}_{GB}(k_s, t)$ that are associated with the stimulated emission (R_1 and R_2) and ground-state bleaching (R_3 and R_4) terms, respectively, i.e.

$$P^{(3)}(k_s, t) = P^{(3)}_{SE}(k_s, t) + P^{(3)}_{GB}(k_s, t) \tag{18}$$

where

$$P^{(3)}_{SE}(k_s, t) \propto \frac{-i\pi E_{pr}(t)}{(\Omega^2 + w^2)^{1/2}\left(\Omega^2 - \frac{H^2(\tau)}{\Omega^2 + w^2} + \bar{w}^2\right)^{1/2}} \exp(-X^2) \left\{\exp(-Y^2(\tau)) + \frac{2i}{\sqrt{\pi}}F(Y(\tau))\right\} \tag{19}$$

$$P^{(3)}_{GB}(k_s, t) \propto \frac{-i\pi E_{pr}(t)}{(\Omega^2 + w^2)^{1/2}\left(\Omega^2 - \frac{H^2(\tau)}{\Omega^2 + w^2} + \bar{w}^2\right)^{1/2}} \exp(-X^2) \left\{\exp(-Z^2(\tau)) + \frac{2i}{\sqrt{\pi}}F(Z(\tau))\right\} \tag{20}$$

Here, the auxiliary functions in eqs 19 and 20 are defined as

$$X \equiv \frac{\omega_{pu} - \omega_{eg}}{\sqrt{2[\Omega^2 + w^2]}}$$

$$Y(\tau) \equiv \frac{\omega_{pr} - \omega_{eg} - 2Q(\tau) - \frac{H(\tau)}{\Omega^2 + w^2}(\omega_{pu} - \omega_{eg})}{\sqrt{2\left(\Omega^2 - \frac{H^2(\tau)}{\Omega^2 + w^2} + \bar{w}^2\right)}}$$

$$Z(\tau) \equiv \frac{\omega_{pr} - \omega_{eg} - \frac{H(\tau)}{\Omega^2 + w^2}(\omega_{pu} - \omega_{eg})}{\sqrt{2\left(\Omega^2 - \frac{H^2(\tau)}{\Omega^2 + w^2} + \bar{w}^2\right)}} \tag{21}$$

The Dawson integral, $F(x)$, in eqs 19 and 20 is defined as[21]

$$F(x) = e^{-x^2}\int_0^x du\, e^{u^2} \tag{22}$$

The spectral diffusion contributions to the particle and hole dynamics on the excited and ground states, respectively, are manifest in eqs 21; note that the time evolutions of centers and variances of Gaussian-approximated particle and hole wave packets are described by the two τ-dependent functions, $Y(\tau)$ and $Z(\tau)$ (see Appendix for a more detailed description on the hole spectral diffusion and for comparison with previous formulation by Mukamel and co-workers[16,20]). For a two-level system, only the two contributions, $P^{(3)}_{SE}(k_s, t)$ and $P^{(3)}_{GB}(k_s, t)$, to the PP polarization are to be considered, whereas for a three-level system, there is an additional contribution, $P^{(3)}_{TA}(k_s, t)$, from the transient absorption (TA) process involving a transition from the first excited state to the second excited state (see section IV below).

Equations 18 with 19 and 20 constitute the principal results of the present section. Because of the τ-dependent terms in eqs 19 and 20, the third-order PP polarization measurement provides information on the spectral diffusion induced by the chromophore-solvent dynamics.

Now, the homodyne-detected TG and heterodyne-detected TD and TB signals can be calculated and found to be

$$S_{TG}(\omega_{pu}, \omega_{pr}; \tau) \propto \int_{-\infty}^{\infty} dt\, |P^{(3)}(k_s, t)|^2 \propto \frac{\exp(-2X^2)}{(\Omega^2 + w^2)\left(\Omega^2 - \frac{H^2(\tau)}{\Omega^2 + w^2} + \bar{w}^2\right)} \left\{[\exp(-Y^2(\tau)) + \exp(-Z^2(\tau))]^2 + \frac{4}{\pi}[F(Y(\tau)) + F(Z(\tau))]^2\right\} \tag{23a}$$

$$S_{TD}(\omega_{pu}, \omega_{pr}; \tau) \propto \mathrm{Im}\left[\int_{-\infty}^{\infty} dt\, E^*_{pr}(k_{pr}, t)P_{PP}(k_s, t; T)\right] \propto \frac{-\exp(-X^2)}{(\Omega^2 + w^2)^{1/2}\left(\Omega^2 - \frac{H^2(\tau)}{\Omega^2 + w^2} + \bar{w}^2\right)^{1/2}} \{\exp(-Y^2(\tau)) + \exp(-Z^2(\tau))\} \tag{23b}$$

$$S_{TB}(\omega_{pu}, \omega_{pr}; \tau) \propto \mathrm{Re}\left[\int_{-\infty}^{\infty} dt\, E^*_{pr}(k_{pr}, t)P_{PP}(k_s, t; T)\right] \propto \frac{\exp(-X^2)}{(\Omega^2 + w^2)^{1/2}\left(\Omega^2 - \frac{H^2(\tau)}{\Omega^2 + w^2} + \bar{w}^2\right)^{1/2}} \left\{\frac{2}{\sqrt{\pi}}F(Y(\tau)) + \frac{2}{\sqrt{\pi}}F(Z(\tau))\right\} \tag{23c}$$

A similar theoretical expression for the TD signal of a two-level system in eq 23b was also obtained by Mukamel and co-workers,[16,20] though they used a different procedure. More specifically, in the high-temperature limit, eq 23b becomes identical to eq 13.32 in ref 16. Their results were later used by others, and particularly, Zhang and Berg showed that the solvation correlation function can be determined by fitting the so-called single-wavelength transient hole burning signal.[23] In the following section, we will examine the above approximate expressions by numerically calculating line shapes in the two-dimensional frequency (ω_{pu} and ω_{pr}) domain.

III. Two-Dimensional Line Shapes: Two-Electronic-Level System

To numerically calculate various 2-D spectra, both the spectral density, $\rho(\omega)$, and the solvent reorganization energy, λ, should be determined first. In the present paper, we will assume that

$$\rho(\omega) \propto \frac{1}{\omega}\exp(-\omega/\omega_c)$$

$$\lambda = 600\ \mathrm{cm}^{-1} \tag{24}$$

Here, the cutoff frequency ω_c is assumed to be 30 cm^{-1}. If the high-temperature approximation is invoked, the mean square fluctuation amplitude, Ω^2, of the electronic transition frequency is approximately calculated to be $\Omega^2 \cong 2\lambda k_B T = 2.48 \times 10^5$ cm^{-2}, which is close to the value $\Omega^2 = 2.49 \times 10^5$ cm^{-2} from eq 16. The normalized solvation correlation function, $S(\tau)/S(0)$, in eq 12 is plotted in Figure 2 (the spectral distribution function, $\omega^2\rho(\omega)$, is also plotted in the inset of Figure 2). The auxiliary function, $H(\tau)$, given in eq 14 is almost indistinguishable from $S(\tau)$ except for a constant factor of $2/\hbar\beta$. The solvation correlation time defined as

$$\tau_{sol} \equiv \int_0^{\infty} d\tau\, S(\tau)/S(0) \tag{25}$$

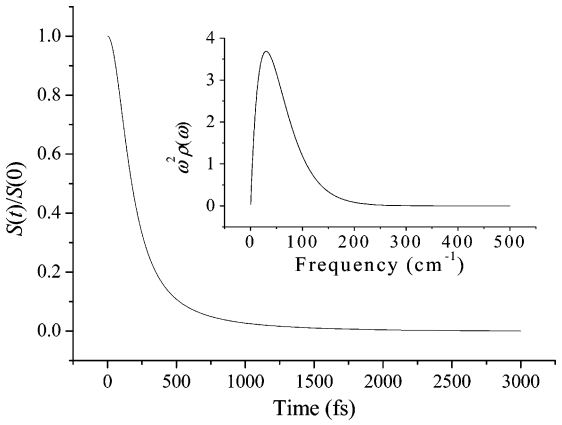

Figure 2. Normalized solvation correlation function, $S(t)/S(0)$, obtained from the spectral density, $\rho(\omega)$, defined in eq 24 is plotted in this figure. The spectral distribution, $\omega^2\rho(\omega)$, is shown in the inset.

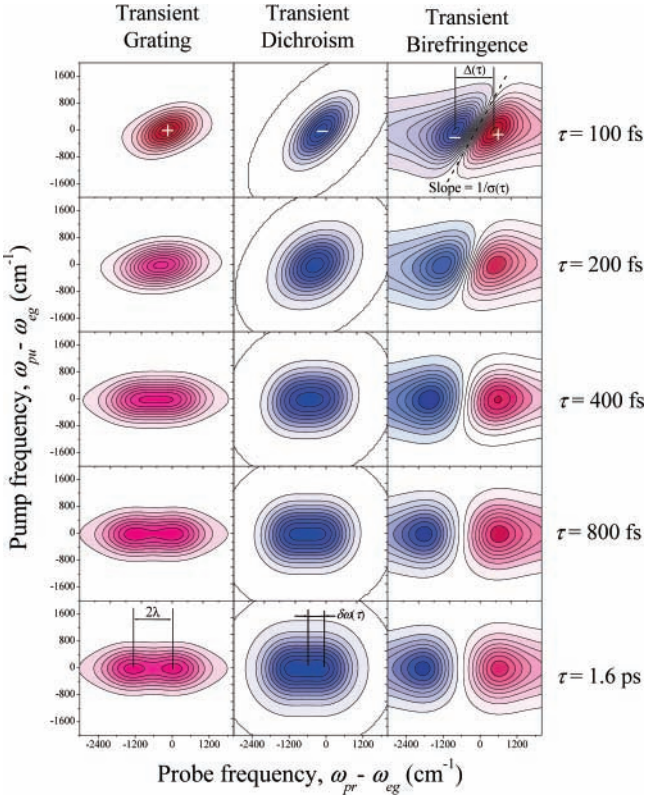

Figure 3. 2-D TG, TD, and TB contours of a two-level system. The five figures in the first column are those of 2-D TG spectra. Those of 2-D TD and 2-D TB spectra are plotted in the second and third columns, respectively. The pump−probe delay time τ, is 100, 200, 400, 800, or 1600 fs.

is estimated to be 262 fs in the case of the present model. Finally, the pump pulse envelop is assumed to be identical to that of the probe pulse, and the full-width at half-maximum (fwhm) of each pulse is set to be 50 fs so that w and $\bar{w}$ are 250 cm^{-1}.

In Figure 3, the three sets of 2-D spectra are plotted. The five contours in the first column correspond to the 2-D TG spectra at the delay time of 100, 200, 400, 800, and 1600 fs, respectively. The contours in the second and third columns are those of 2-D TD and TB spectra. Throughout the present paper, the population relaxation contribution to the signals that can be taken into account by multiplying an exponentially decaying function to eqs 23 will be ignored not because it is not important but because it does not change the 2-D line shapes.

First of all, the shapes of the TG and TD spectra at τ less than 800 fs are observed to be tilted. Particularly, the TD spectrum at $\tau = 100$ fs is diagonally elongated. The degree of slant of the TG and TD contours decreases as the pump−probe pulse delay time increases. The reason the 2-D TG and TD spectra are significantly slant in the short time region is because the memory on the phase space of the initially pumped wave packet does not decay down to zero in such a short time. This memory loss rate is determined by the function, $H(\tau)$, defined in eq 11, or approximately the solvation correlation function, $S(\tau)$.

Second, there appear two separated peaks in the 2-D TG spectra at $\tau = 800$ and 1600 fs (see the bottom two figures in the first column of Figure 3). The peak separation is estimated to be $2\lambda = 1200$ cm^{-1}. This can be easily understood by noting that the TD and TG signals in the limit of large delay time are given by a sum of two 2-D Gaussian functions centered at ($\omega_{pu} = \omega_{eg}$, $\omega_{pr} = \omega_{eg}$) and ($\omega_{pu} = \omega_{eg}$, $\omega_{pr} = \omega_{eg} - 2\lambda$) and its square, respectively, (see eqs 23a and 23b), i.e.

$$S_{TG}(\tau \to \infty) \approx \frac{\exp(-2X^2)}{(\Omega^2 + w^2)(\Omega^2 + \bar{w}^2)}\{[\exp(-Y^2(\infty)) + \exp(-Z^2(\infty))]^2\}$$

$$S_{TD}(\tau \to \infty) \approx \frac{\exp(-X^2)}{(\Omega^2 + w^2)^{1/2}(\Omega^2 + \bar{w}^2)^{1/2}}\{\exp(-Y^2(\infty)) + \exp(-Z^2(\infty))\} \quad (26)$$

where

$$Y(\infty) \equiv \frac{\omega_{pr} - \omega_{eg} + 2\lambda/\hbar}{\sqrt{2(\Omega^2 + \bar{w}^2)}}$$

$$Z(\infty) \equiv \frac{\omega_{pr} - \omega_{eg}}{\sqrt{2(\Omega^2 + \bar{w}^2)}} \quad (27)$$

Here, the transient birefringence (the real part of the polarization) contribution to the TG signal becomes negligibly smaller than the transient dichroism (the imaginary part of the polarization) contribution so that in the long time limit the TG signal becomes directly proportional to the square of the TD signal. On the basis of the above observation about the τ-dependent peak separation of the TD spectrum, one can experimentally measure the spectral diffusion process dictated by the solvation correlation function, $S(\tau)$. One complicating factor is that the two peaks are not clearly frequency-resolved in the short time region so that this method may not be useful for extracting information on the early part of the solvation correlation function. This situation is very similar to the photon echo peak shift (PEPS) measurement. As was shown by Cho et al.,[15] the PEPS is linearly proportional to the solvation correlation function in the long time region, though the initial decaying part of the PEPS is obscured by complicated contributions intrinsically associated with the short-time nonlinear response function of the photon echo spectroscopy. To overcome this difficulty, Skinner and co-workers theoretically showed that the initial slope of the photon echo signal is linearly proportional to $S(\tau)$.[19,20] Although it is likely to be complicated due to the pulse overlap effects, it can be an alternative way to extract quantitative information on the solvation correlation function.

As can be seen in the five figures in the second column of Figure 3, the center position of the 2-D TD spectrum changes with respect to the pulse delay time and its location is at (ω_{pu}

$= \omega_{eg}$ and $\omega_{pr} = \omega_{eg} + \delta\omega(\tau)$), where the τ-dependent frequency shift $\delta\omega(\tau)$ is found to be

$$\delta\omega(\tau) = Q(\tau) = S(\tau) - \frac{\lambda}{\hbar} \tag{28}$$

Therefore, it was shown that the τ-dependent $\delta\omega(\tau)$ obtained from the centers of TD spectra can directly provide quantitative information on the solvation correlation function, $S(\tau)$.

Now, let us consider the 2-D TB spectra shown in the third column of Figure 3. As expected, each spectrum contains both positive and negative peaks. Note that the two peaks at the maximum and the minimum are separated from each other and the magnitude of peak separation, $\Delta(\tau)$, increases as the pump−probe pulse delay time increases (see the top right figure for the definition of $\Delta(\tau)$). Unlike the cases of TG and TD, the approximate expression for the TB spectrum in eq 23c is not just a sum of two 2-D Gaussian functions so that it is not straightforward to obtain an expression for the relationship between $\Delta(\tau)$ and $S(\tau)$. However, we found another interesting feature exhibited by the 2-D TB spectra. In the region between the two (positive and negative) peaks, the tangential line of the 2D contours (the dotted line in the top right panel of Figure 3) is slant in the short time region. Let's denote the inverse slope of this linear line (the dotted line in Figure 3) as $\sigma(\tau)$. As the pump−probe delay time increases, $\sigma(\tau)$ approaches zero. This trend can be theoretically explained by using the approximate expression for the 2-D TB spectrum. By considering the contour of $S_{TB}(\omega^*_{pu},\omega^*_{pr};\ \tau) = 0$; the slope of the tangential line of this specific contour in the region between the positive and negative peaks can be estimated as follows. First of all, the middle position between these two peaks has to be determined for this purpose. Because the Dawson's integral, $F(x)$, reaches a maximum value at $x = 0.92$,[21] $|F(Y(\tau))|$ and $|F(Z(\tau))|$ become maximum when, for $\omega_{pu} = \omega_{eg}$

$$\frac{\omega_{pr} - \omega_{eg} - 2Q(\tau)}{\sqrt{2\left(\Omega^2 - \frac{H^2(\tau)}{\Omega^2 + w^2} + \bar{w}^2\right)}} = 0.92 \quad \text{and}$$

$$\frac{\omega_{pr} - \omega_{eg}}{\sqrt{2\left(\Omega^2 - \frac{H^2(\tau)}{\Omega^2 + w^2} + \bar{w}^2\right)}} = 0.92 \tag{29}$$

respectively. Therefore, the location of the midpoint between the positive and negative peaks is at

$$\omega^*_{pu}(0) = \omega_{eg} \quad \text{and} \quad \omega^*_{pr}(0) = 0.92\sqrt{2\left(\Omega^2 - \frac{H^2(\tau)}{\Omega^2 + w^2} + \bar{w}^2\right)} + \omega_{eg} + Q(\tau) \tag{30}$$

To calculate the slope of the tangential line (see the dotted line in the top right panel of Figure 3), consider the case when the pump field frequency is slightly increased from ω_{eg} by δ, the location of the midpoint shifts to

$$\omega^*_{pu}(\delta) = \omega_{eg} + \delta \quad \text{and} \quad \omega^*_{pr}(\delta) = 0.92\sqrt{2\left(\Omega^2 - \frac{H^2(\tau)}{\Omega^2 + w^2} + \bar{w}^2\right)} + \omega_{eg} + Q(\tau) + \frac{H(\tau)}{\Omega^2 + w^2}\delta. \tag{31}$$

Consequently, the inverse slope of the tangential line, denoted as $\sigma(\tau)$, is found to be

$$\sigma(\tau) = \frac{\omega^*_{pr}(\delta) - \omega^*_{pr}(0)}{\delta} = \frac{H(\tau)}{\Omega^2 + w^2} \cong \left(\frac{2}{\hbar\beta}\right)\frac{S(\tau)}{\Omega^2 + w^2} \tag{32}$$

This result suggests that one can directly obtain the solvation correlation function by measuring the degree of slant of 2-D TB contours as a function of τ. In the long time domain, it will be very difficult to measure an entire 2-D spectrum because of weakness and noise of the signal. In this case, for a given delay time τ, one can instead measure two 1-D TB spectra (as a function of ω_{pr}) at two different fixed pump frequencies such as $\omega_{pu} = \omega_{eg}$ and $\omega_{pu} = \omega_{eg} + \delta$. Then, the first equality of eq 32 can be used to determine $\sigma(\tau)$ (or equally $S(\tau)$) value in the long time domain.

Finally, a brief discussion on the static inhomogeneity contribution to the 2-D TG, TD, and TB spectra is presented. Although there is no truly static inhomogeneity in solution, chromophores in a glassy material or a polymer matrix would have inhomogeneous environments. In the case of the PEPS measurement, the asymptotic value of the PEPS does not vanish when there are sufficiently slow processes. Then, what are the signatures of the static inhomogeneity in the 2-D TG, TD, and TB spectra? If the static distribution is a Gaussian with standard deviation of Σ (in cm^{-1}), one should simply perform the following replacements in eqs 23

$$\Omega^2 \rightarrow \Omega^2 + \Sigma^2$$

$$H(\tau) \rightarrow H(\tau) + \Sigma^2 \tag{33}$$

where the units of Ω and $\sqrt{H(\tau)}$ are transformed into cm^{-1}. In this case of a finite inhomogeneity system, the 2-D TG and TD contours remain to be slant regardless of the pump−probe pulse delay time. Furthermore, the 2-D TB contour would not be vertically directed even in the long-time domain; note that the contours shown in the bottom right panel of Figure 3 are vertically directed at $\tau = 1.6$ ps because that is the case of $\Sigma = 0$. Thus, if an asymptotic value of the experimentally measured inverse slope, $\sigma(\tau \rightarrow \infty)$, would approach to a finite value, it could be a strong signature that there is a finite inhomogeneous contribution to the line broadening. Moreover, the asymptotic value, $\sigma(\tau \rightarrow \infty)$, is directly related to the width of the static inhomogeneity as

$$\sigma(\tau \rightarrow \infty) = \frac{\Sigma^2}{\Omega^2 + \Sigma^2 + w^2} \tag{34}$$

Using this relationship, one can quantitatively determine Σ.

IV. Two-Dimensional Line Shapes: Three-Vibrational-Level System

In sections II and III, we only considered TG, TD, and TB signals of a two-electronic-level system. Recently, an IR pump−probe technique has been extensively used to study amide I vibrational dynamics of various short polypeptides.[24−30] In this case, not only the first vibrationally excited state but also the second excited state is involved in the pump−probe four-wave-mixing process. For instance, the IR photon echo and IR pump−probe experiments for an *N*-methylacetamide-D (NMAD) dissolved in liquid D_2O were carried out by Hochstrasser and co-workers[31] and Hamm and co-workers,[13] respectively. Another example of an application of the IR four-wave-mixing spectroscopies was to study hydrogen-bonding dynamics in liquid

water. The O−H(D) stretching vibration is anharmonic, and it was observed that its frequency is strongly dependent on the hydrogen-bond distance.[32−38] Again, in this case, the molecular system can be approximated to be a three-vibrational-level system.

A. PP Polarization of a Three-Level System. To understand the role of solvation (H-bond) dynamics in the nonlinear molecular response to multiple IR fields, we recently carried out molecular dynamics simulation studies in combination with ab initio calculation methods. Particularly, the amide I vibration of the NMA was studied in detail. In this case, one should at least consider three vibrational levels denoted as $|g\rangle$, $|e\rangle$, and $|f\rangle$, where $|f\rangle$ is the overtone (second excited) state. For such a three-level system, we shall first present a generalized version of the 2-D TG, TD, and TB signals by adding an additional contribution, the so-called transient absorption term. As shown in Figure 1, two more Feynman diagrams denoted as R_5 and R_6 should be included to calculate the total polarization. In ref 39, a general expression for nonlinear response function of any arbitrary multi-level system was presented.[39,40] The corresponding two response function components associated with R_5 and R_6 are found to be

$$\begin{aligned}R_5(t_3, t_2, t_1) = &-\langle \mu_{eg}{}^2 \mu_{fe}{}^2 \rangle \exp\{-i\omega_{fe} t_3 + \\ &i\omega_{eg} t_1\} \exp\{-\int_{t_1}^{t_1+t_2} d\tau_1 \int_{t_1}^{\tau_1} d\tau_2\, \xi_{ee}(\tau_1, \tau_2) - \\ &\int_{t_1+t_2}^{t_1+t_2+t_3} d\tau_1 \int_{t_1+t_2}^{\tau_1} d\tau_2\, \xi_{ff}(\tau_1, \tau_2) - \\ &\int_{0}^{t_1+t_2+t_3} d\tau_1 \int_{0}^{\tau_1} d\tau_2\, \xi^*_{ee}(\tau_1, \tau_2) - \\ &\int_{t_1}^{t_1+t_2} d\tau_1 \int_{t_1+t_2}^{t_1+t_2+t_3} d\tau_2\, \xi^*_{ef}(\tau_1, \tau_2) + \\ &\int_{t_1}^{t_1+t_2} d\tau_1 \int_{0}^{t_1+t_2+t_3} d\tau_2\, \xi^*_{ee}(\tau_1, \tau_2) + \\ &\int_{t_1+t_2}^{t_1+t_2+t_3} d\tau_1 \int_{0}^{t_1+t_2+t_3} d\tau_2\, \xi^*_{fe}(\tau_1, \tau_2)\}\end{aligned}$$

$$\begin{aligned}R_6(t_3, t_2, t_1) = &-\langle \mu_{eg}{}^2 \mu_{fe}{}^2 \rangle \exp\{-i\omega_{fe} t_3 - \\ &i\omega_{eg} t_1\} \exp\{-\int_{0}^{t_1+t_2} d\tau_1 \int_{0}^{\tau_1} d\tau_2\, \xi_{ee}(\tau_1, \tau_2) - \\ &\int_{t_1+t_2}^{t_1+t_2+t_3} d\tau_1 \int_{t_1+t_2}^{\tau_2} d\tau_2\, \xi_{ff}(\tau_1, \tau_2) - \\ &\int_{t_1}^{t_1+t_2+t_3} d\tau_1 \int_{t_1}^{\tau_1} d\tau_2\, \xi^*_{ee}(\tau_1, \tau_2) - \\ &\int_{0}^{t_1+t_2} d\tau_1 \int_{t_1+t_2}^{t_1+t_2+t_3} d\tau_2\, \xi^*_{ef}(\tau_1, \tau_2) + \\ &\int_{0}^{t_1+t_2} d\tau_1 \int_{t_1}^{t_1+t_2+t_3} d\tau_2\, \xi^*_{ee}(\tau_1, \tau_2) + \\ &\int_{t_1+t_2}^{t_1+t_2+t_3} d\tau_1 \int_{t_1}^{t_1+t_2+t_3} d\tau_2\, \xi^*_{fe}(\tau_1, \tau_2)\} \quad (35)\end{aligned}$$

The orientational average of the transition dipole product was denoted as $\langle \mu_g{}^2 \mu_{fe}{}^2 \rangle$ in eqs 35. In the case of a weakly anharmonic oscillator, $\langle \mu_{eg}{}^2 \mu_{fe}{}^2 \rangle \cong 2\langle \mu_{eg}{}^4 \rangle$. Unlike the case of a two-level system, in addition to the linear correlation function $\xi_{ee}(\tau_2)$ defined in eq 7, it is necessary to determine three more linear correlation functions such as

$$\begin{aligned}\xi_{ff}(\tau_2) &= \langle \delta\omega_{fg}(\tau_2) \delta\omega_{fg}(0) \rangle \\ \xi_{ef}(\tau_2) &= \langle \delta\omega_{eg}(\tau_2) \delta\omega_{fg}(0) \rangle \\ \xi_{fe}(\tau_2) &= \langle \delta\omega_{fg}(\tau_2) \delta\omega_{eg}(0) \rangle \end{aligned} \quad (36)$$

where $\delta\omega_{fg}$ is the fluctuating part of the transition frequency from $|g\rangle$ to $|f\rangle$ states. For a weakly anharmonic oscillator, if the solute−solvent interaction causes fluctuation of the vibrational force constant, one can assume that

$$\delta\omega_{fg}(t) \cong 2\delta\omega_{eg}(t) \quad (37)$$

Then, the three correlation functions in eqs 36 can be related to $\xi_{ee}(\tau_2)$ as

$$\xi_{ee}(\tau_2) = \frac{1}{4}\xi_{ff}(\tau_2) = \frac{1}{2}\xi_{ef}(\tau_2) = \frac{1}{2}\xi_{fe}(\tau_2). \quad (38)$$

Using these relationships, we can rewrite the two transient absorption components in eqs 35 as, in terms of the line broadening function $g(t)$

$$\begin{aligned}R_5(t_3, t_2, t_1) = &-\langle \mu_{eg}{}^2 \mu_{fe}{}^2 \rangle \exp\{-i\omega_{fe} t_3 + i\omega_{eg} t_1\} \\ &\exp\{-g(t_3) - g^*(t_1) + g(t_2) - g^*(t_1 + t_2) - g(t_2 + t_3) + \\ &g^*(t_1 + t_2 + t_3)\}\end{aligned}$$

$$\begin{aligned}R_6(t_3, t_2, t_1) = &-\langle \mu_{eg}{}^2 \mu_{fe}{}^2 \rangle \exp\{-i\omega_{fe} t_3 - i\omega_{eg} t_1\} \\ &\exp\{-g(t_3) - g(t_1) - g^*(t_2) + g(t_1 + t_2) + g^*(t_2 + t_3) - \\ &g(t_1 + t_2 + t_3)\} \quad (39)\end{aligned}$$

By using the same procedure and approximations discussed in section II, the transient absorption contribution to the material polarization, $P^{(3)}_{\mathrm{TA}}(k_s, t)$, is found to be

$$\begin{aligned}P^{(3)}_{\mathrm{TA}}(k_s, t) \propto &\frac{2i\pi E_{\mathrm{pr}}(t)}{(\Omega^2 + w^2)^{1/2}\left(\Omega^2 - \dfrac{H^2(\tau)}{\Omega^2 + w^2} + \bar{w}^2\right)^{1/2}} \exp(-X^2) \\ &\left\{\exp(-W^2(\tau)) + \frac{2i}{\sqrt{\pi}} F(W(\tau))\right\} \quad (40)\end{aligned}$$

where

$$W(\tau) \equiv \frac{\omega_{\mathrm{pr}} - \omega_{\mathrm{fe}} - 2Q(\tau) - \dfrac{H(\tau)}{\Omega^2 + w^2}(\omega_{\mathrm{pu}} - \omega_{\mathrm{eg}})}{\sqrt{2\left(\Omega^2 - \dfrac{H^2(\tau)}{\Omega^2 + w^2} + \bar{w}^2\right)}} \quad (41)$$

Note that $P^{(3)}_{\mathrm{TA}}(k_s, t)$ differs from $P^{(3)}_{\mathrm{SE}}(k_s, t)$ by (i) the factor of -2 and (ii) $\omega_{\mathrm{pr}} - \omega_{\mathrm{eg}} \rightarrow \omega_{\mathrm{pr}} - \omega_{\mathrm{fe}}$.

Therefore, for a three-vibrational-level system, the total PP polarization is given as a sum of three contributions

$$P^{(3)}(k_s, t) = P^{(3)}_{\mathrm{SE}}(k_s, t) + P^{(3)}_{\mathrm{GB}}(k_s, t) + P^{(3)}_{\mathrm{TA}}(k_s, t) \quad (42)$$

Because of the phase difference between $P^{(3)}_{\mathrm{TA}}(k_s, t)$ and $P^{(3)}_{\mathrm{SE}}(k_s, t) + P^{(3)}_{\mathrm{GB}}(k_s, t)$, the additional transient absorption contribution interferes destructively in the region where the spectral overlap is large. Using eq 42, we find that the 2-D TG, TD, and TB signals are

$$S_{TG}(\omega_{pu}, \omega_{pr}; \tau) \propto \frac{\exp(-2X^2)}{(\Omega^2 + w^2)\left(\Omega^2 - \frac{H^2(\tau)}{\Omega^2 + w^2} + \bar{w}^2\right)} \left\{[\exp(-Y^2(\tau)) + \exp(-Z^2(\tau)) - 2\exp(-W^2(\tau))]^2 + \frac{4}{\pi}[F(Y(\tau)) + F(Z(\tau)) - 2F(W(\tau))]^2\right\}$$

$$S_{TD}(\omega_{pu}, \omega_{pr}; \tau) \propto \frac{\exp(-X^2)}{(\Omega^2 + w^2)^{1/2}\left(\Omega^2 - \frac{H^2(\tau)}{\Omega^2 + w^2} + \bar{w}^2\right)^{1/2}} \{2\exp(-W^2(\tau)) - \exp(-Y^2(\tau)) - \exp(-Z^2(\tau))\}$$

$$S_{TB}(\omega_{pu}, \omega_{pr}; \tau) \propto \frac{\exp(-X^2)}{(\Omega^2 + w^2)^{1/2}\left(\Omega^2 - \frac{H^2(\tau)}{\Omega^2 + w^2} + \bar{w}^2\right)^{1/2}} \left\{\frac{2}{\sqrt{\pi}}F(Y(\tau)) + \frac{2}{\sqrt{\pi}}F(Z(\tau)) - \frac{4}{\sqrt{\pi}}F(W(\tau))\right\} \quad (43)$$

B. Numerical Calculations. To study how the 2-D TG, TD, and TB spectra change by the addition of the transient absorption contribution, they were numerically calculated for a model three-level system. First of all, the functional form of the spectral density, $\rho(\omega)$, will be assumed to be the same with eq 24, but the solvent reorganization energy, λ, is set to be 10 cm^{-1}. Note that the vibrational Stokes shift is typically tens or hundreds of times smaller than the electronic Stokes shift. If the high-temperature approximation were invoked, the mean square fluctuation amplitude, Ω^2, of the vibrational transition frequency would be approximately calculated to be $\Omega^2 \cong 2\lambda k_B T = 4140$ cm^{-2}. The IR pump pulse envelop is assumed to be identical to that of the IR probe pulse and the full-width at half-maximum (fwhm) of each pulse is set to be 200 fs so that w and $\bar{w}$ are 63 cm^{-1}.

Because of the nonzero vibrational anharmonicity, we assume that the frequency difference $\delta\omega_{anh} = \omega_{eg} - \omega_{fe}$ is 30 cm^{-1}. Now, the three sets of calculated 2-D spectra for the TG, TD, and TB signals are plotted in Figure 4. The delay time varies as 200, 400, 800, 1200, and 1600 fs. The 2-D TG spectrum at $\tau = 200$ fs is slightly slant, but that at $\tau = 1600$ fs is symmetric. Other than the tilted contours, the 2-D TG spectra are featureless.

Next, let us consider the 2-D TD spectra shown in the middle column of Figure 4. The transient absorption contribution to the signal is positive and appears as the left peak in a 2-D TD spectrum, whereas the negative peak appearing on the right corresponds to the sum of stimulated emission and ground-state bleaching contributions. The reason the two peaks are separated from each other is because of the nonzero anharmonicity, i.e., $\omega_{eg} - \omega_{fe} = 30$ cm^{-1}, and of partial destructive interference between them. However, the peak separation is found to be about 180 cm^{-1}, which is much larger than the anharmonicity of 30 cm^{-1}. Furthermore, the two peak positions, though they are functions of τ via $Q(\tau)$, along the ω_{pr} axis and the magnitude of peak separation do not change much with respect to τ. Thus, a question is immediately raised: what determines the peak separation in the 2-D TD spectra? To provide a quantitative answer to this question, it should be first noted that the two contributions, $2\exp(-W^2(\tau))$ and $-\exp(-Y^2(\tau)) - \exp(-Z^2(\tau))$, at $\omega_{pu} = \omega_{eg}$ are Gaussian functions centered at $\omega_{pr} = \omega_{eg} - \delta\omega_{anh} + 2Q(\tau)$ and $\omega_{pr} = \omega_{eg} + Q(\tau)$, respectively. The maximum values of $2\exp(-W^2(\tau))$ and $\exp(-Y^2(\tau)) + \exp(-Z^2(\tau))$ are in this case almost the same. Thus, the slice of the 2-D TD spectrum at $\omega_{pu} = \omega_{eg}$ can be recast in the form

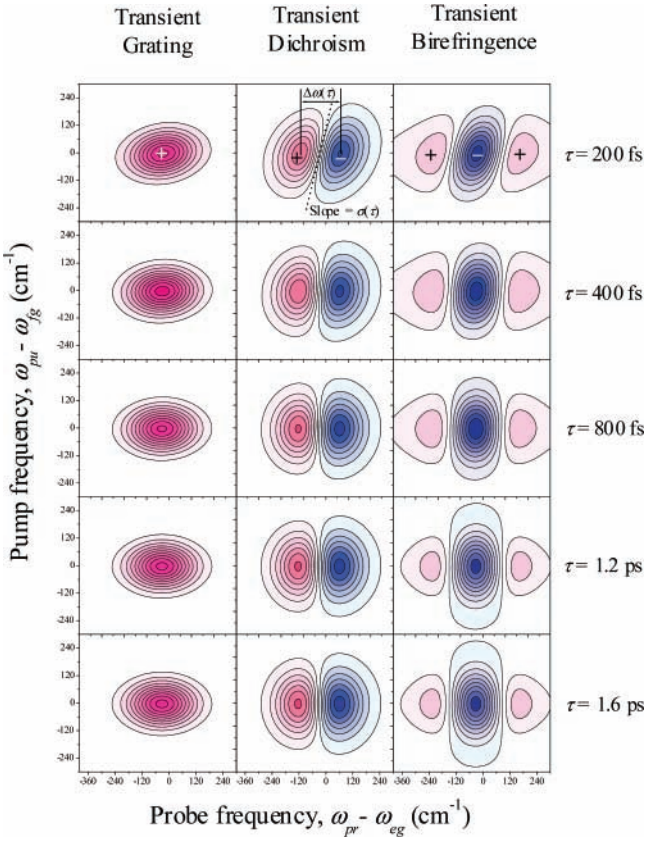

Figure 4. 2-D TG, TD, and TB contours of a three-level system. The five figures in the first column are those of 2-D TG spectra. Those of 2-D TD and 2-D TB spectra are plotted in the second and third columns, respectively. The pump−probe delay time τ, is 200, 400, 800, 1200, or 1600 fs.

$$S_{TD}(\omega_{pu} = \omega_{eg}, \omega_{pr}; \tau) \propto \exp(-A(\tau)\{x - x_1(\tau)\}^2) - \exp(-A(\tau)\{x - x_2(\tau)\}^2) \quad (44)$$

where

$$x \equiv \omega_{pr} - \omega_{eg}$$

$$x_1(\tau) \equiv 2Q(\tau) - \delta\omega_{anh}$$

$$x_2(\tau) \equiv Q(\tau)$$

$$A(\tau) \equiv \frac{1}{2(\Omega^2 - H^2(\tau)[\Omega^2 + w^2]^{-1} + \bar{w}^2)} \quad (45)$$

The two (positive and negative) peak positions can be found by solving the following nonlinear equation, obtained from $\partial S_{TD}(\omega_{pu} = \omega_{eg}, \omega_{pr}; \tau)\}/\partial x = 0$, for x

$$\frac{x - x_1(\tau)}{x - x_2(\tau)} = \exp\{-A(\tau)[2(x_1(\tau) - x_2(\tau))x - x_1^2(\tau) + x_2^2(\tau)]\} \quad (46)$$

One cannot analytically solve the above nonlinear equation to find two roots. However, noting that, regardless of τ, for x in

the range from $[x_1(\tau) + x_2(\tau)]/2 - (\Omega^2 + \bar{w}^2)^{1/2}$ to $[x_1(\tau) + x_2(\tau)]/2 + (\Omega^2 + \bar{w}^2)^{1/2}$

$$|A(\tau)[2(x_1(\tau) - x_2(\tau))x]| \ll 1 \tag{47}$$

one can approximately rewrite eq 46 as a quadratic equation of $(\omega_{pr} - \omega_{eg})$. Thus, the magnitude of the peak separation, denoted as $\Delta\omega(\tau)$ in Figure 4, is approximately found to be

$$\Delta\omega(\tau) \cong \sqrt{4(\Omega^2 - H^2(\tau)[\Omega^2 + w^2]^{-1} + \bar{w}^2) + Q^2(\tau)} \tag{48}$$

which, in this case, varies from 175 to 180 cm^{-1} as τ increases from 200 to 1600 fs. Ignoring the τ-dependent terms in eq 48, we further simplify it as $\Delta\omega \cong 2(\Omega^2 + \bar{w}^2)^{1/2}$, which is 180 cm^{-1}. This is close to the numerical result. Thus, it is concluded that, if the square root of $\Omega^2 + \bar{w}^2$ is larger than the sum of $\delta\omega_{anh}$ and $\lambda/\hbar$, or in other words if the two peaks are strongly overlapped, the magnitude of peak separation in a 2-D TD spectrum of a three-level system is determined not by the anharmonicity but by the root-mean-square fluctuation amplitude and spectral bandwidth of the probe pulse, i.e., $\Delta\omega(\tau) \cong 2(\Omega^2 + \bar{w}^2)^{1/2}$, as long as $\delta\omega_{anh} \neq 0$. This is the case studied in the present section, e.g., $(\Omega^2 + \bar{w}^2)^{1/2} = 90$ cm^{-1} and $\delta\omega_{anh} + \lambda/\hbar = 40$ cm^{-1}.

Second, the degree of slant of the 2-D TD contours is an interesting feature that should be studied in detail. Much like the case of the 2-D TB spectrum of a two-level system, the 2-D TD contours of a three-level system studied in this section are not vertically directed. Defining $\sigma(\tau)$ to be the inverse slope of the tangential line of the contours at ($\omega_{pu} = \omega_{eg}$ and $\omega_{pr} = \omega_{eg} + [x_1(\tau) + x_2(\tau)]/2$), we find

$$\sigma(\tau) = \frac{H(\tau)}{\Omega^2 + w^2} \cong \left(\frac{2}{\hbar\beta}\right)\frac{S(\tau)}{\Omega^2 + w^2} \tag{49}$$

Again, once the inverse slope, $\sigma(\tau)$, is experimentally measured as a function of τ, the solvation correlation function can be obtained by using the above relationship, eq 49.

Now, consider 2-D TB spectra plotted in the third column of Figure 4. Because of the interference between the transient absorption polarization and the sum of stimulated emission and ground-state bleaching polarizations, the 2-D TB spectrum exhibits an up−down−up feature. The 2-D contours are again slant when the pump−probe pulse delay time, τ, is not sufficiently larger than the solvation correlation time, τ_{sol}.

Similar to the case of two-level systems, the static inhomogeneity effects on various PP spectra of three-level systems can be understood by performing the same replacements summarized in eq 33. Again, the asymptotic value of the inverse slope, $\sigma(\tau \rightarrow \infty)$, will give us information on the existence and magnitude of static inhomogeneity.

V. Summary

In the present paper, theoretical descriptions of two-color TG, TD, and TB spectroscopies were presented for both two- and three-level systems. It was shown that the 2-D line shapes are strongly dependent on the solvation dynamics. In particular, for a two-level system, the 2-D TB contours appear not to be vertically directed when the pump−probe pulse delay time is not sufficiently larger than the solvation correlation time. Also, it was shown that the delay-time-dependent 2-D TG and TD spectra can provide quantitative information on the reorganization energy and spectral diffusion dynamics. For a three-level system, we obtained approximate expressions for the 2-D TG, TD, and TB spectral profiles. The peak separation in a 2-D TD spectrum was found to be determined by the fluctuation amplitude of transition frequency and spectral bandwidth of the probe pulse. Similar to the case of 2-D TB of a two-level system, the 2-D TD contours of a three-level system were found to be slant for a short time. The inverse slope of the tilted tangential line was found to be linearly proportional to the solvation correlation function. Overall, the approximate expressions for the 2-D pump−probe signals presented in this paper will be of use in the investigations of pure dephasing, static inhomogeneity, and chromophore-solvent dynamics of two- and three-level systems. One can use the same theory to describe IR four-wave-mixing spectroscopies of any multi-level systems because the corresponding response function can be decomposed into those of three-level systems and the material polarization would be expressed as a sum of them. Currently, we are applying the present theory to the calculations of IR PP spectra of short polypeptides in solution.

Acknowledgment. This work was supported by the Creative Research Initiative Program of KISTEP (KOSEF, Korea). We thank Mr. Prall and Prof. Fleming for stimulating discussions and sharing their unpublished experimental results with us.

Appendix: Spectral Diffusion of a Ground-State Hole

Although R_3 and R_4 in eq 17 appear not to incorporate spectral diffusion of ground-state bleach ("hole") because of the absence of $Q(\tau)$ terms in the short-time approximated expressions for R_3 and R_4, the ground-state hole is also subject to the spectral diffusion of which time-dependence is described by the function $H(\tau)$; note that both $H(\tau)$ and $Q(\tau)$ are linearly proportional to $S(\tau)$ in the high-temperature limit. As can be seen in eq 20, the τ−dependence of $P^{(3)}_{GB}(k_s, t)$, which is the polarization associated with the ground-state bleaching contribution, is determined by the auxiliary function $Z(\tau)$, i.e.

$$Z(\tau) \equiv \frac{\omega_{pr} - \omega_{eg} - \dfrac{H(\tau)}{\Omega^2 + w^2}(\omega_{pu} - \omega_{eg})}{\sqrt{2\left(\Omega^2 - \dfrac{H^2(\tau)}{\Omega^2 + w^2} + \bar{w}^2\right)}} \tag{21}$$

The variance of this hole wave packet as well as the center frequency of this 2-D Gaussian function, i.e., $\exp(-Z^2(\tau))$, both depend on the pump−probe delay time, τ. To directly compare our expression with eq 13.32 in ref 16, let us rewrite $Z(\tau)$ as

$$Z(\tau) \equiv \frac{\omega_{pr} - \omega_g(\tau)}{\sqrt{2\alpha(\tau)}} \tag{A1}$$

where

$$\omega_g(\tau) \equiv \omega_{eg} + \frac{H(\tau)}{\Omega^2 + w^2}(\omega_{pu} - \omega_{eg}) \tag{A2}$$

$$\alpha(\tau) \equiv \Omega^2 - \frac{H^2(\tau)}{\Omega^2 + w^2} + \bar{w}^2 \tag{A3}$$

Here, it should be noted that ω_{eg}, in the present paper, is the frequency at the absorption maximum so that it differs from that in ref 16, where ω_{eg} denoted the 0−0 transition frequency. If we replace ω_{eg} in eqs 21 and 23b with $\omega^0_{eg} - \lambda$, the similarity between our results and Mukamel's expression for the TD signal of a two-level system is manifest; note that eq 13.32 corresponds to the high-temperature limit of our eq 23b.

From eq A2, it is clear that, only in the case when $\omega_{pu} = \omega_{eg}$, there is no spectral diffusion of a ground-state hole. Otherwise, a hole would also spectrally shift in time and its dynamics is dictated by $H(\tau)$.

References and Notes

(1) Fayer, M. D. *Annu. Rev. Phys. Chem.* **1982**, *33*, 63.
(2) Andrews, J. R.; Hochstrasser, R. M. *Chem. Phys. Lett.* **1980**, *76*, 213.
(3) Deeg, F. W.; Fayer, M. D. *J. Chem. Phys.* **1989**, *91*, 2269.
(4) Fourkas, J. T.; Fayer, M. D. *Acc. Chem. Res.* **1992**, *25*, 227.
(5) Goldberg, S. Y.; Bart, E.; Meltsin, A.; Fainberg, B. D.; Huppert, D. *Chem. Phys.* **1994**, *183*, 217.
(6) Joo, T.; Jia, Y.; Yu, J.-Y.; Lang, M.; Fleming, G. R. *J. Chem. Phys.* **1996**, *104*, 6089.
(7) Xu, Q. H.; Ma, Y. Z.; Fleming, G. R. *J. Phys. Chem. A* **2002**, *106*, 10755.
(8) Fleming, G. R. private communication. In the paper Agarwal, R.; Prall, B. S.; Rizvi, A. H.; Yang, M.; Fleming, G. R. *J. Chem. Phys.* **2002**, *116*, 6243, the first two-color photon echo peak shift measurement was reported and theoretically described.
(9) Cho, M.; Fleming, G. R. *J. Phys. Chem.* **1994**, *98*, 3478.
(10) Hybl, J. D.; Albrecht, A. W.; Gallagher Faeder, S. M.; Jonas, D. M. *Chem. Phys. Lett.* **1998**, *297*, 307. Hybl, J. D.; Yu, A.; Farrow, D. A.; Jonas, D. M. *J. Phys. Chem. A* **2002**, *106*, 7651.
(11) Tokmakoff, A. *J. Phys. Chem. A* **2000**, *104*, 4247.
(12) Woutersen, S.; Hamm, P. *J. Phys. Chem.* **2000**, *104*, 11316.
(13) Woutersen, S.; Pfister, R.; Hamm, P.; Mu, Y.; Kosov, D. S.; Stock, G. *J. Chem. Phys.* **2002**, *117*, 6833.
(14) Kwac, K.; Cho, M. *J. Chem. Phys.* **2003**, in press.
(15) Cho, M.; Yu, J.-Y.; Joo, T.; Nagasawa, Y.; Passino, S. A.; Fleming, G. R. *J. Phys. Chem.* **1996**, *100*, 11944.
(16) Mukamel, S. *Principles of Nonlinear Optical Spectroscopy*; Oxford University Press: Oxford, U.K., 1995.
(17) Cho, M.; Fleming, G. R.; Mukamel, S. *J. Chem. Phys.* **1993**, *98*, 5314.
(18) Fleming, G. R.; Cho, M. *Annu. Rev. Phys. Chem.* **1996**, *47*, 103.
(19) Everitt, K. F.; Geva, E.; Skinner, J. L. *J. Chem. Phys.* **2001**, *114*, 1326.
(20) Piryatinski, A.; Skinner, J. L. *J. Phys. Chem. B* **2002**, *106*, 8055.
(21) *Handbook of Mathematical Functions with Formulas, Graphs, and Mathematical Tables*; Abramowitz, M., Stegun, I. A., Eds.; Dover Publications: New York, 1974.
(22) Loring, R. F.; Yan, Y. J.; Mukamel, S. *J. Chem. Phys.* **1987**, *87*, 5840. Yan, Y. J.; Mukamel, S. *Phys. Rev. A* **1990**, *41*, 6485.
(23) Zhang, Y.; Berg, M. A. *J. Chem. Phys.* **2001**, *115*, 4223.
(24) Hamm, P.; Lim, M.; Hochstrasser, R. M. *J. Phys. Chem. B* **1998**, *102*, 6123.
(25) Hamm, P.; Lim, M.; Degradon, W. F.; Hochstrasser, R. M. *Proc. Natl. Acad. Sci. U.S.A.* **1999**, *96*, 2036.
(26) Hamm, P.; Lim, M.; Degrado, W. F.; Hochstrasser, R. M. *J. Chem. Phys.* **2000**, *112*, 1907.
(27) Woutersen, S.; Hamm, P. *J. Phys. Chem. B* **2000**, *104*, 11316.
(28) Woutersen, S.; Hamm, P. *J. Chem. Phys.* **2001**, *115*, 7737.
(29) Woutersen, S.; Mu, Y.; Stock, G.; Hamm, P. *Proc. Natl. Acad. Sci. U.S.A.* **2001**, *98*, 11254.
(30) Rubtsov, I. V.; Hochstrasser, R. M. *J. Phys. Chem. B* **2002**, *106*, 9165.
(31) Zanni, M. T.; Asplund, M. C.; Hochstrasser, R. M. *J. Chem. Phys.* **2001**, *114*, 4579.
(32) Graener, H.; Seifert, G.; Laubereau, A. *Phys. Rev. Lett.* **1991**, *66*, 2092.
(33) Laenen, R.; Rauscher, C.; Laubereau, A. *Phys. Rev. Lett.* **1998**, *80*, 2622.
(34) Woutersen, S.; Bakker, H. *Phys. Rev. Lett.* **1999**, *83*, 2077.
(35) Gale, G. M.; Gallot, G.; Hache, F.; Lascoux, N. *Phys. Rev. Lett.* **1999**, *82*, 1068.
(36) Bratos, S.; Gale, G. M.; Gallot, G.; Hache, F.; Lascoux, N.; Leicknam, J.-Cl. *Phys. Rev. E* **2000**, *61*, 5211.
(37) Stenger, J.; Madsen, D.; Hamm, P.; Nibbering, E. T. J.; Elsaesser, T. *Phys. Rev. Lett.* **2001**, *87*, 027401.
(38) Stenger, J.; Madsen, D.; Hamm, P.; Nibbering, E. T. J.; Elsaesser, T. *J. Phys. Chem. A* **2002**, *106*, 2341.
(39) Cho, M. *J. Chem. Phys.* **2001**, *115*, 4424.
(40) Sung, J.; Silbey, R. J. *J. Chem. Phys.* **2001**, *115*, 9266.